

UC Irvine

UC Irvine Previously Published Works

Title

Evidence for multi-decadal fuel buildup in a large California wildfire from smoke radiocarbon measurements

Permalink

<https://escholarship.org/uc/item/17x898zk>

Journal

Environmental Research Letters, 18(9)

ISSN

1748-9318

Authors

Odwuor, A
Yañez, CC
Chen, Y
et al.

Publication Date

2023-09-01

DOI

10.1088/1748-9326/aced17

Peer reviewed

LETTER • OPEN ACCESS

Evidence for multi-decadal fuel buildup in a large California wildfire from smoke radiocarbon measurements

To cite this article: A Odwuor *et al* 2023 *Environ. Res. Lett.* **18** 094030

View the [article online](#) for updates and enhancements.

You may also like

- [The effect of particulate matter on solar photovoltaic power generation over the Republic of Korea](#)
Junghoon Son, Sujong Jeong, Hayoung Park *et al.*
- [Pollution characteristics and influencing factors of atmospheric particulate matter \(PM_{2.5}\) in Chang-Zhu-Tan area](#)
Yong Zhang and Wulin Jiang
- [Natural ventilation versus air pollution: assessing the impact of outdoor pollution on natural ventilation potential in informal settlements in India](#)
Kopal Nihar, Alex Nutkiewicz and Rishee K Jain

ENVIRONMENTAL RESEARCH
LETTERS

LETTER

OPEN ACCESS

RECEIVED
9 March 2023REVISED
19 June 2023ACCEPTED FOR PUBLICATION
3 August 2023PUBLISHED
24 August 2023

Original content from
this work may be used
under the terms of the
[Creative Commons
Attribution 4.0 licence](#).

Any further distribution
of this work must
maintain attribution to
the author(s) and the title
of the work, journal
citation and DOI.



Evidence for multi-decadal fuel buildup in a large California wildfire from smoke radiocarbon measurements

A Odwuor^{1,*} , C C Yañez¹ , Y Chen¹ , F M Hopkins² , A Moreno^{2,3} , X Xu¹ , C I Czimczik¹ and J T Randerson¹ ¹ Department of Earth System Science, University of California, Irvine, CA, United States of America² Department of Environmental Sciences, University of California, Riverside, CA, United States of America³ California Air Resources Board, Riverside, CA, United States of America

* Author to whom any correspondence should be addressed.

E-mail: aodwuor@uci.edu**Keywords:** biomass burning, western U.S. forests, carbon-14, aerosol, ecosystem turnover time**Abstract**

In recent decades, there has been a significant increase in annual area burned in California's Sierra Nevada mountains. This rise in fire activity has prompted the need to understand how historical forest management practices affect fuel composition and emissions. Here we examined the total carbon (TC) concentration and radiocarbon abundance ($\Delta^{14}\text{C}$) of particulate matter (PM) emitted by the KNP Complex Fire, which occurred during California's 2021 wildfire season and affected several groves of giant sequoia trees in the southern Sierra Nevada. During a 26 h sampling period, we measured concentrations of fine airborne PM ($\text{PM}_{2.5}$), as well as dry air mole fractions of carbon monoxide (CO) and methane (CH_4), using a ground-based mobile laboratory. We also collected filter samples of $\text{PM}_{2.5}$ for analysis of TC concentration and $\Delta^{14}\text{C}$. High correlation among $\text{PM}_{2.5}$, CO, and CH_4 time series confirmed that our $\text{PM}_{2.5}$ measurements captured variability in wildfire emissions. Using a Keeling plot approach, we determined that the mean $\Delta^{14}\text{C}$ of $\text{PM}_{2.5}$ was $111.6 \pm 7.7\text{‰}$ ($n = 12$), which was considerably enriched relative to atmospheric carbon dioxide in the northern hemisphere in 2021 ($-3.2 \pm 1.4\text{‰}$). Combining these $\Delta^{14}\text{C}$ data with a steady-state one-box ecosystem model, we estimated that the mean age of fuels combusted in the KNP Complex Fire was 40 years, with a range of 29–57 years. These results provide evidence for emissions originating from woody biomass, larger-diameter fine fuels, and coarse woody debris that have accumulated over multiple decades. This is consistent with independent field observations that indicate high fire intensity contributed to widespread giant sequoia mortality. With the expanded use of prescribed fires planned over the next decade in California to mitigate wildfire impacts, our measurement approach has the potential to provide regionally-integrated estimates of the effectiveness of fuel treatment programs.

1. Introduction

Wildfire activity in California, including area burned and occurrence of large fires, has increased over the last several decades, with intensifying impacts on society, the economy, and ecosystems (Dennison *et al* 2014, Williams *et al* 2019, Safford *et al* 2022, Wang *et al* 2021). During high fire years, mandatory evacuation orders force tens of thousands of people to flee their homes (Safford *et al* 2022). Direct costs of wildfires, including fire suppression and property losses, have more than doubled in the

last decade (California Department of Forestry and Wildfire Protection, 2022a). Wildfires also incur significant indirect costs (Wang *et al* 2021) like environmental cleanup, lost business revenue, infrastructure repair, and health impacts. Wildfires account for up to half of the exposure to $\text{PM}_{2.5}$ (airborne particulate matter (PM) with diameter $<2.5 \mu\text{m}$) in the western U.S. (Burke *et al* 2021), and smoke exposure has been linked to increased respiratory-related hospitalizations and adverse health outcomes related to restricted activity and days of work lost (Kochi *et al* 2010, Reid *et al* 2016). California's ecosystems

are also negatively affected by intensifying wildfires, which can weaken landscape-scale carbon storage, shift vegetation composition, reduce biodiversity, and threaten water supplies and other ecosystem services (Wu *et al* 2011, Stevens 2017a, Foster *et al* 2020). These worsening impacts motivate an urgent need for research aimed at informing and evaluating wildfire management strategies in California and the western U.S.

In the Sierra Nevada mountains of California, burned area has increased by more than seven-fold since the 1980s, mainly as a consequence of the cumulative effects of widespread fire suppression and climate change (Taylor *et al* 2016, Williams *et al* 2019, Gutierrez *et al* 2021, Hagmann *et al* 2021). Widespread suppression of low- to moderate-intensity fires has allowed overgrowth of shrubs and small trees, which compete with larger trees for resources (e.g. water) and serve as ladder fuels that facilitate high-intensity crown fires (McKelvey and Busse 1996, Stephens *et al* 2009, Pausas and Keeley 2019). In addition to fuel buildup, the region has experienced warmer and drier conditions that increase the likelihood of more frequent and extensive wildfires (Williams *et al* 2019, Abatzoglou *et al* 2021, Gutierrez *et al* 2021, Higuera and Abatzoglou 2021).

Although California's coniferous trees evolved with fire and can withstand low- to moderate-intensity fires with a return interval of about 15 years (Swetnam 1993, Swetnam *et al* 2009), they are vulnerable to today's high-intensity crown fires (Shive *et al* 2022). This is especially important to consider in old-growth forests, such as stands of the endangered giant sequoia (*Sequoiadendron giganteum*, (LINDL.) J.T. BUCHHOLZ), which have experienced widespread mortality in recent higher-intensity fires (Shive *et al* 2022). Specifically, fires like the Castle Fire in 2020 and KNP Complex Fire in 2021 contributed to giant sequoia mortality. The Castle Fire killed an estimated 10%–14% of large (>1.2 m dbh) sequoias (Stephenson and Brigham 2021, Shive *et al* 2022). Today's fire regime is unlike what California's forests and communities have experienced in the past (Stevens *et al* 2021), motivating greater investments in forest and wildfire management practices, including prescribed fire, to reduce fire severity (Tubbesing *et al* 2021).

In this study, we measured the radiocarbon abundance ($\Delta^{14}\text{C}$; Stuvier and Polach 1977) of $\text{PM}_{2.5}$ emitted by the KNP Complex Fire over a 26 h sampling period, along with *in situ* trace gas dry air mole fractions and $\text{PM}_{2.5}$ concentrations, which were used to validate the influence of wildfire emissions on variability in observed $\text{PM}_{2.5}$ concentrations. We then used this information to constrain the ages (and types) of combusted fuels and explore implications for fire intensity. Radiocarbon (^{14}C) is a radioactive isotope of carbon that is naturally produced in the atmosphere. Still, the $\Delta^{14}\text{C}$ of atmospheric carbon dioxide (CO_2) has changed considerably over the past

70 years because of the Earth system's response to the production of 'bomb' ^{14}C from aboveground nuclear weapons testing during the late 1950s and early 1960s (Nydal 1963, Levin *et al* 2010). In past work, $\Delta^{14}\text{C}$ measurements of fire-emitted PM have been used to identify the depth of burning in organic duff layers in boreal forest ecosystems (Mouteva *et al* 2015) and the age of combusted peats contributing to severe haze events in Southeast Asia (Wiggins *et al* 2018). For western U.S. wildfires, $\Delta^{14}\text{C}$ measurements can provide information about the size classes of combusted fuels because larger-diameter fuels decompose more slowly and, therefore, persist longer within ecosystems (Harmon 2021).

We hypothesized that fire-emitted $\text{PM}_{2.5}$ would be considerably enriched in ^{14}C relative to current atmospheric CO_2 because larger-diameter fuels incorporated ^{14}C via photosynthesis over several decades when the atmosphere had more bomb ^{14}C . Older fuels are associated with larger fuel classes, which decompose relatively slowly and build up for decades if not removed mechanically or by fire. Several methods are commonly used to assess fire severity, including the composite burn index (Key and Benson 2006) and remotely-sensed indices, like the normalized burn ratio (Miller *et al* 2009a). Measuring the $\Delta^{14}\text{C}$ of fire emissions may complement these approaches by constraining the age (and therefore, size distribution) of combusted fuels. By sampling the atmosphere downwind of a large wildfire, our technique also provides a means to obtain a regionally-integrated snapshot across actively burning areas within the entire fire perimeter.

2. Methods

2.1. Sampling location

We collected $\text{PM}_{2.5}$ samples and measured *in situ* trace gas and $\text{PM}_{2.5}$ levels with a ground-based mobile laboratory in the town of Three Rivers, CA, USA (36.453°N, 118.873°W, 361 m above sea level) during 2–3 October 2021. We chose this sampling location to be as close to the KNP Complex Fire as possible without being inside a mandatory evacuation zone. This was within a residential community approximately 0.5 km from the town's main road. Traffic was minimal because the area was under an evacuation warning. Our sampling location was about 10 km from two actively burning fire fronts that were located to the north and east and approximately 1000 m lower in elevation. The KNP Complex Fire resulted from two lightning fires (Colony and Paradise Fires) that merged into one large fire on 17 September 2021 (Stephenson and Brigham 2021). The fire was 100% contained on 16 December 2021 after reaching a final size of 357 km² (88 307 acres) (California Department of Forestry and Fire Protection 2022b). Over the course of the fire, it burned 18 km² (4374 acres) of giant sequoia groves (Shive *et al* 2022).

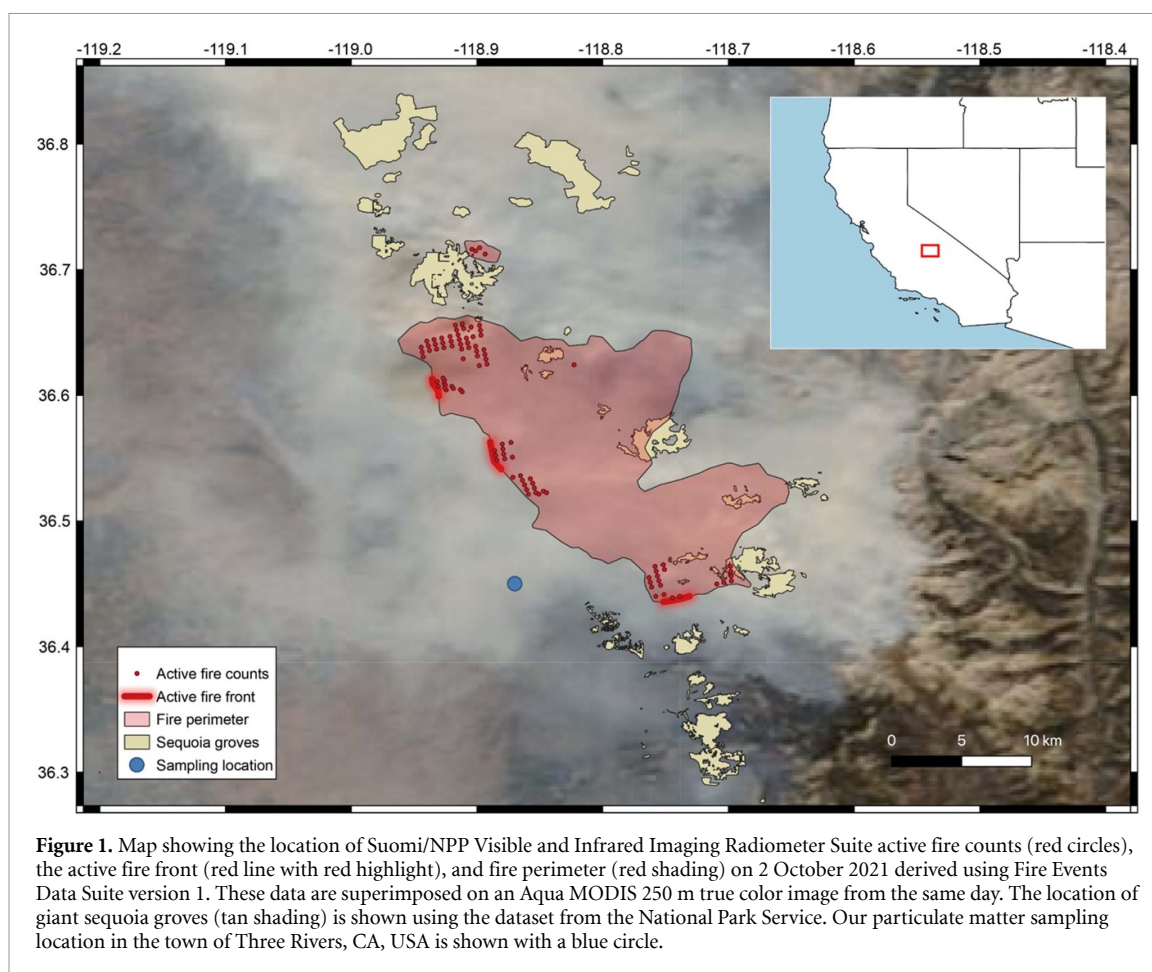


Figure 1 shows our sampling location and the distribution of Suomi/NPP Visible and Infrared Imaging Radiometer Suite active fires for the 1:30 pm overpass on 2 October. The active fire line and outer fire perimeter for the KNP Complex Fire on 2 October are also mapped using information from the Fire Events Data Suite version 1 (Chen *et al* 2022). This fire information is superimposed on an Aqua MODIS 250 m true color image displaying the spatial extent of smoke from the KNP Complex Fire on 2 October. The location of giant sequoia groves is also provided using data from the National Park Service (National Park Service and Sequoia and Kings Canyon National Parks 2017). Three lines of evidence confirmed our sampling location was downwind of the fire and its plume: (1) elevated and covarying trace gas and $PM_{2.5}$ concentrations (as described in Results), (2) visual inspection of the smoke cloud in figure 1 and (3) back-trajectory analysis conducted with NOAA's HYSPLIT model (data not shown).

Air temperature and relative humidity reported here were measured by a compact weather sensor (METSSENS500, Campbell Scientific, Logan, UT, USA) mounted on the mobile laboratory approximately 3 m above ground level. The air temperature was 32.0 °C at the beginning of the sampling period at 3:00 pm on 2 October and declined through the evening and night, reaching a minimum of 17.4 °C at

7:45 am on 3 October. The temperature rose through the morning and afternoon on 3 October, reaching a maximum of 27.2 °C at 2:25 pm. Relative humidity varied from 14% to 26% over the sampling period, within the minimum observed at 3:00 pm on 2 October and the maximum at 26% at 10:30 am on 3 October.

2.2. $PM_{2.5}$ measurement and collection

We measured *in situ* $PM_{2.5}$ mass concentrations ($\mu g PM_{2.5} m^{-3}$ air) using a PurpleAir PA-II air quality sensor with laser particle counting (PurpleAir, Draper, UT, USA) at a sampling height of approximately 1.2 m above ground. We analyzed the PurpleAir Channel A data, which is appropriate for outdoor conditions and has a 2 min resolution.

Filter samples of $PM_{2.5}$ were collected at an inlet height of 1.2 m above ground level using a low-volume aerosol sampler (MiniVol Tactical Air Sampler, AirMetrics, Springfield, OR, USA) with a $PM_{2.5}$ impactor (#202-100) over periods of 0.5–6.0 h. Sampling duration was determined according to concurrent $PM_{2.5}$ concentration (i.e., sampling duration was inversely related to concurrent $PM_{2.5}$ concentration). To maintain a uniform volume flow, we used ambient temperature and pressure to adjust the sampler's flow rate between 4.50 and 4.75 l min^{-1} . Samples were collected on 47 mm diameter quartz

fiber filters (GE Healthcare Life Sciences, #1851-047). Before sampling, filters were pre-combusted at 500 °C for 3 h, wrapped individually in aluminum foil, and stored in plastic bags. Blank filters were mounted on the inside of the sampler housing with no active airflow and collected concurrently with 2 of the 12 PM_{2.5} samples (#253740 and 253744). After collection, filters were wrapped in aluminum foil, sealed in plastic bags, and stored at −20 °C. A total of 12 PM_{2.5} samples and 2 blanks were collected.

2.3. Elemental and isotopic analyses of PM_{2.5}

2.3.1. Measurement of TC and radiocarbon

Filter samples of PM_{2.5} were analyzed for TC concentration ($\mu\text{g C m}^{-3}$) and $\Delta^{14}\text{C}$ at the W. M. Keck Carbon Cycle Accelerator Mass Spectrometry (KCCAMS) laboratory at the University of California, Irvine. We focused our analysis on the $\Delta^{14}\text{C}$ of PM_{2.5} because it is a criteria pollutant for the U.S. Environmental Protection Agency (EPA) and is associated with a wide range of particles generated during combustion (Andreae 2019). Examining fuel age, PM_{2.5} presents various practical advantages: it is conveniently sampled in the field and in wildfire smoke, and its relatively high signal-to-noise ratio enables a clear differentiation from the background atmosphere.

For each sample, a portion of or the entire filter (depending on estimated TC concentration) was sealed with cupric oxide in pre-combusted 6 mm OD quartz tubes and oxidized to CO₂ at 900 °C for 3 h. This TC-derived CO₂ was then extracted and quantified manometrically on a vacuum line, reduced to graphite using a modified sealed-tube zinc reduction method (Walker and Xu 2019), and its $\Delta^{14}\text{C}$ was measured via accelerator mass spectrometry

alongside graphitization standards and blanks. The units of $\Delta^{14}\text{C}$ are per mille (‰), and the relationship between $\Delta^{14}\text{C}$ and the widely-used fraction modern (F) measurement is shown in equation (1), where y is the year of ¹⁴C sampling (2021); F is the ¹⁴C/¹²C ratio of the sample divided by 95% of the ¹⁴C/¹²C ratio of the oxalic acid I (OX-I) standard measured in 1950 ($^{14}\text{C}/^{12}\text{C}_{\text{OXI}} = 1.176 \pm 0.010 \times 10^{-12}$) corrected for mass-dependent fractionation; 8267 years is the mean lifetime of ¹⁴C; and 1950 is the reference year,

$$\Delta^{14}\text{C} = \left(F \times e^{\frac{1950-y}{8267}} - 1 \right) \times 1000. \quad (1)$$

The ¹⁴C data are normalized to a common $\delta^{13}\text{C}$ so that differences in $\Delta^{14}\text{C}$ do not reflect isotopic fractionation processes (Stuvier and Polach 1977).

TC and $\Delta^{14}\text{C}$ measurements for our PM_{2.5} samples are reported in table 1. Error in TC was computed assuming 3% error in sampler flow rate, 0.5% error in sampling duration, and 6% error in our measurement of the filter area. The measured $\Delta^{14}\text{C}$ of each sample ($\Delta^{14}\text{C}_{\text{meas}}$) was corrected for contamination by extraneous carbon associated with handling the filters during field and laboratory work using blank filters and a simple isotopic mass balance equation (equation (2)):

$$\Delta^{14}\text{C}_{\text{sample}} = \frac{\Delta^{14}\text{C}_{\text{meas}} \times \text{TC}_{\text{meas}} - \Delta^{14}\text{C}_{\text{blank}} \times \text{TC}_{\text{blank}}}{\text{TC}_{\text{meas}} - \text{TC}_{\text{blank}}} \quad (2)$$

where ‘sample’ refers to the sampled filter and ‘blank’ refers to the blank filter. The mean blank TC concentration was 0.1 $\mu\text{g C cm}^{-2}$, and the blank mean $\Delta^{14}\text{C}$ was $-278.6 \pm 14.3\text{‰}$. The error (*err*) in $\Delta^{14}\text{C}_{\text{sample}}$ was calculated according to equation (3):

$$\text{err in } \Delta^{14}\text{C}_{\text{sample}} = \sqrt{\left(\frac{\text{TC}_{\text{meas}}}{\text{TC}_{\text{sample}}} \times \text{err in } \Delta^{14}\text{C}_{\text{meas}} \right)^2 - \left(\frac{\text{TC}_{\text{blank}}}{\text{TC}_{\text{sample}}} \times \text{err in } \Delta^{14}\text{C}_{\text{blank}} \right)^2}. \quad (3)$$

2.3.2. Keeling plot analysis

A Keeling plot regression analysis (Keeling 1958, Pataki et al 2003) allows us to estimate the $\Delta^{14}\text{C}$ of the wildfire PM_{2.5} end member, separating it from PM_{2.5} in the background atmosphere (Mouteva et al 2015, Wiggins et al 2018). Application of the Keeling plot equation (equation (4)) draws upon the linear relationship between $\Delta^{14}\text{C}_{\text{sample}}$ and $1/\text{TC}_{\text{sample}}$ and allows for identification of the wildfire $\Delta^{14}\text{C}$ end member from the regression intercept:

$$\Delta^{14}\text{C}_{\text{sample}} = \text{TC}_{\text{background}} \times \left(\Delta^{14}\text{C}_{\text{background}} - \Delta^{14}\text{C}_{\text{wildfire}} \right) \times \frac{1}{\text{TC}_{\text{sample}}} + \Delta^{14}\text{C}_{\text{wildfire}}. \quad (4)$$

The 12 sampled filter measurements of $1/\text{TC}$ and $\Delta^{14}\text{C}$ were fit using a geometric mean regression, which accounts for errors in both TC and $\Delta^{14}\text{C}$ measurements. The regression was calculated using the ‘lsqfitgm’ function in Matlab developed by E. T. Peltzer at the Monterey Bay Aquarium Research

Table 1. Summary of total carbon (TC) concentration and $\Delta^{14}\text{C}$ of $\text{PM}_{2.5}$ collected within the smoke plume of the KNP Complex Fire in Three Rivers, CA, USA. Error in $\text{TC}_{\text{sample}}$ and $\Delta^{14}\text{C}_{\text{sample}}$ represent the propagated uncertainty in the collection of these measurements.

Date	Start (PDT)		End (PDT)		$\text{TC}_{\text{sample}}$ ($\mu\text{g C m}^{-3}$)			$\Delta^{14}\text{C}_{\text{sample}}$ (‰)		UCI AMS #
	Time	Time	Time	Time	Mean	Error	Mean	Error		
2 October 2021	15:10	15:40			1.5	130.6 ± 8.7	−16.8 ± 6.9			253731
2 October 2021	16:09	17:39			3.3	97.5 ± 6.5	−83.6 ± 5.6			253734
2 October 2021	17:53	19:23			3.8	111.7 ± 7.5	−33.7 ± 4.9			253735
2 October 2021	19:38	21:38			8.4	185.9 ± 12.6	34.5 ± 3.0			253736
2 October 2021	21:49	23:49			18.7	392.4 ± 26.6	68.9 ± 1.9			253737
3 October 2021	00:12	04:12			40.8	427.3 ± 28.7	81.0 ± 3.1			253738
3 October 2021	04:24	07:24			29.0	405.4 ± 27.5	78.2 ± 1.9			253739
3 October 2021	07:38	09:38			21.0	439.8 ± 29.6	76.5 ± 1.9			253740
3 October 2021	09:46	12:16			28.4	475.7 ± 32.1	79.9 ± 3.8			253743
3 October 2021	12:28	14:28			25.2	556.4 ± 37.6	72.8 ± 1.9			253744
3 October 2021	14:43	16:13			16.9	497.1 ± 33.5	66.8 ± 2.0			253745
3 October 2021	16:18	17:48			18.3	539.8 ± 36.7	43.4 ± 2.1			253746

Institute⁴. The standard deviation (SD) of wildfire $\Delta^{14}\text{C}$ is the SD of the y -intercept calculated by the regression function. The Keeling plot approach assumes the composition of the wildfire end member and background atmosphere remain constant over the sampling duration.

2.3.3. Estimation of combusted fuel mean age

The mean age of the combusted fuel was determined using a steady-state one-box ecosystem model forced with $\Delta^{14}\text{C}$ of the historical atmosphere using observations by Hua *et al* (2022) and X Xu⁵. Given a user-prescribed mean age of the carbon pool, the model simulates the evolving $\Delta^{14}\text{C}$ of the pool from 10 000 years before present to 2021 with inputs from photosynthesis and losses from decomposition and radioactive decay each year. We ran the model for a range of mean ages (between 5 and 75 years) to simulate the $\Delta^{14}\text{C}$ of the terrestrial carbon pool in 2021. We then matched the mean $\Delta^{14}\text{C}$ of combusted fuel end member from the Keeling plot approach described above (section 2.3.2) to the mean age from the model corresponding to the closest matching $\Delta^{14}\text{C}$ value. We estimated a 1σ uncertainty range for the fuel mean ages by identifying where the measured wildfire $\Delta^{14}\text{C}$ end member value minus 1σ intersected the curve of ecosystem model predictions. This approach generated an asymmetric uncertainty range for the fuel age.

2.4. Trace gas measurements

Carbon monoxide (CO) and methane (CH_4) dry air mole fractions were measured using a wavelength-scanned cavity ring-down spectrometer (G2401, Picarro, Santa Clara, CA, USA) at an inlet height of approximately 3 m above ground at approximately 1 s resolution. We calibrated measurements before

and after the sampling period using two NOAA-certified air standards in compressed gas cylinders with known mole fractions of CO and CH_4 that spanned the range of observed values. Standards were measured for approximately 5 min during the calibration period. Using the linear relationship between known values and values measured during the calibration period, we applied a two-point correction to the CO and CH_4 data obtained during the sampling period (Hopkins *et al* 2016, Yañez *et al* 2022). Outliers in the data (values more than three scaled median absolute deviations from the median) were replaced with linear interpolation of neighboring, non-outlier values using the ‘filloutliers’ function in Matlab⁶. Measurements collected when cavity pressure or temperature in the instrument was unstable (pressure/temperature change between measurements >0) were removed. Calibrated data with outliers removed were then averaged to a 1 min resolution.

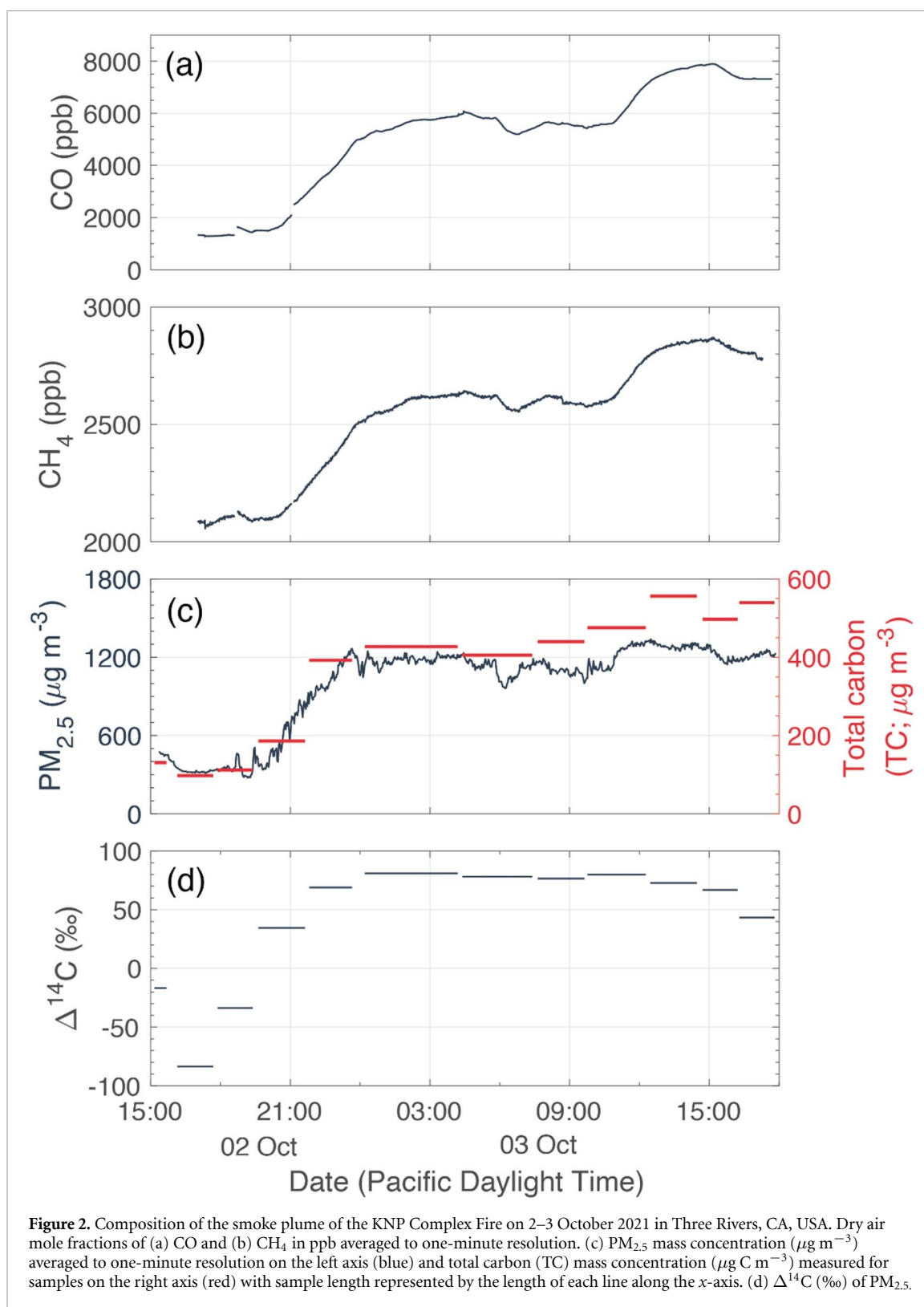
3. Results

Throughout the 26 h sampling period, CO, CH_4 , and $\text{PM}_{2.5}$ measurements varied synchronously and were elevated relative to expected background levels (figure 2). CO near the beginning of the sampling period at 5:10 pm on 2 October was approximately 1330 ppb. CO increased rapidly at first and then more gradually, reaching a level of 6000 ppb around 4:30 am on 3 October (figure 2(a)). CO levels varied between 6000 and 5630 ppb from 4:00 am to 11:00 am on 3 October before increasing again in the early afternoon, reaching a maximum of 7890 ppb by 3:10 pm. CH_4 measurements followed a similar temporal pattern with a minimum initial dry air mole fraction of 2090 ppb at 5:10 pm on 2 October and then increasing to a maximum of 2870 ppb at 3:10 pm on 3 October (figure 2(b)). $\text{PM}_{2.5}$ concentrations increased during the evening of 2 October

⁴ lsqfitgm function by E. T. Peltzer, Monterey Bay Aquarium Research Institute.

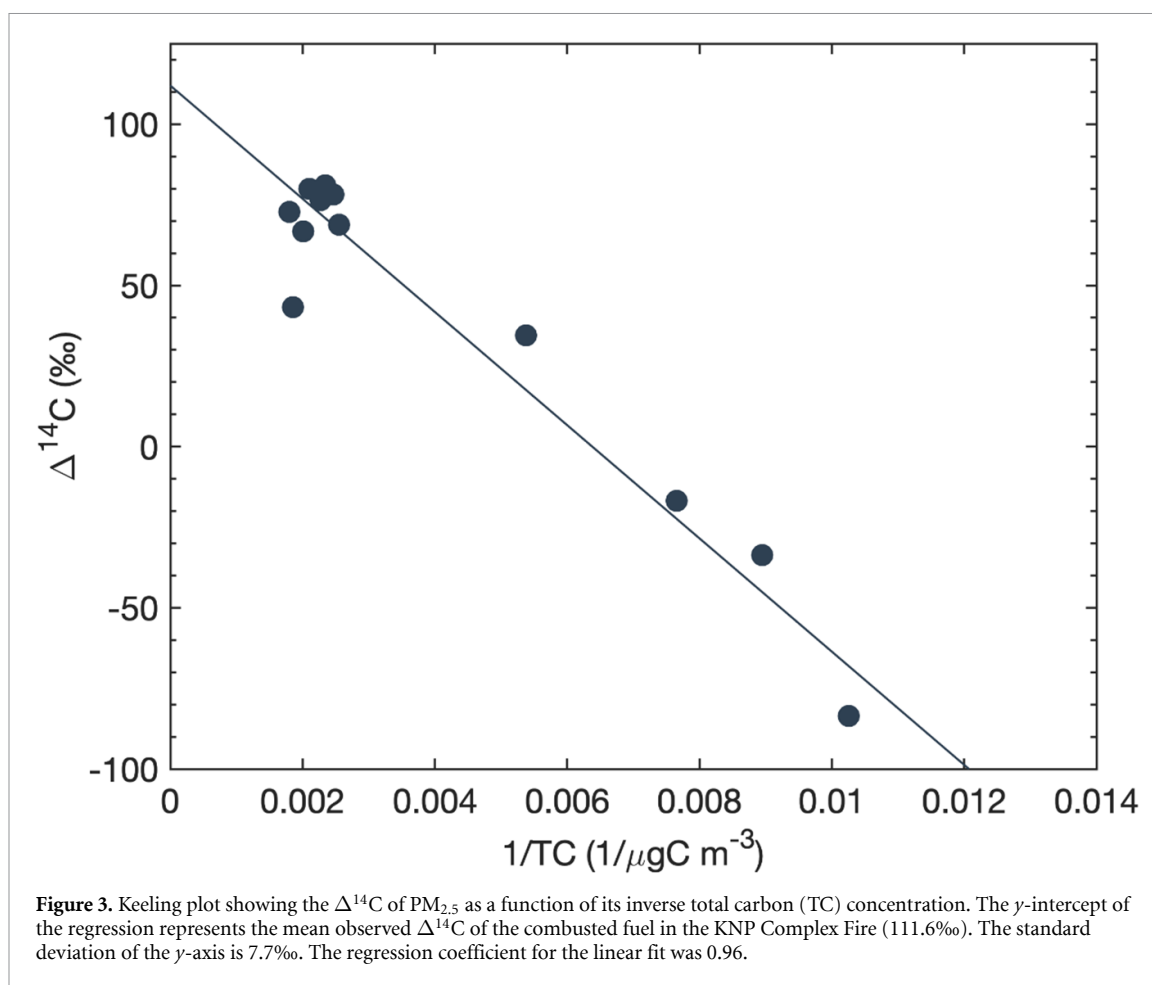
⁵ X. Xu, personal communication 2022.

⁶ filloutliers function Copyright 2016–2021 The MathWorks, Inc.



with similar timing to CO and CH₄. PM_{2.5} remained relatively constant from midnight to 6:15 am on 3 October (figure 2(c)). A minimum in PM_{2.5} concentration of $277 \mu\text{g m}^{-3}$ was observed at 7:20 pm on 2 October and a maximum of $1330 \mu\text{g m}^{-3}$ was observed at 12:25 pm on 3 October. Compared to CO and CH₄, PM_{2.5} had a much less pronounced rise in the early afternoon on 3 October. The Pearson

correlation coefficients for the different trace gas and PM_{2.5} time series were relatively high: 0.99 for CO and CH₄, 0.91 for CO and PM_{2.5}, and 0.90 for CH₄ and PM_{2.5}. The simultaneous buildup of fire-emitted PM_{2.5} and trace gases during the evening and night of 2 October is consistent with a collapsing planetary boundary layer and downslope flow from the fire to our lower elevation sampling location, which

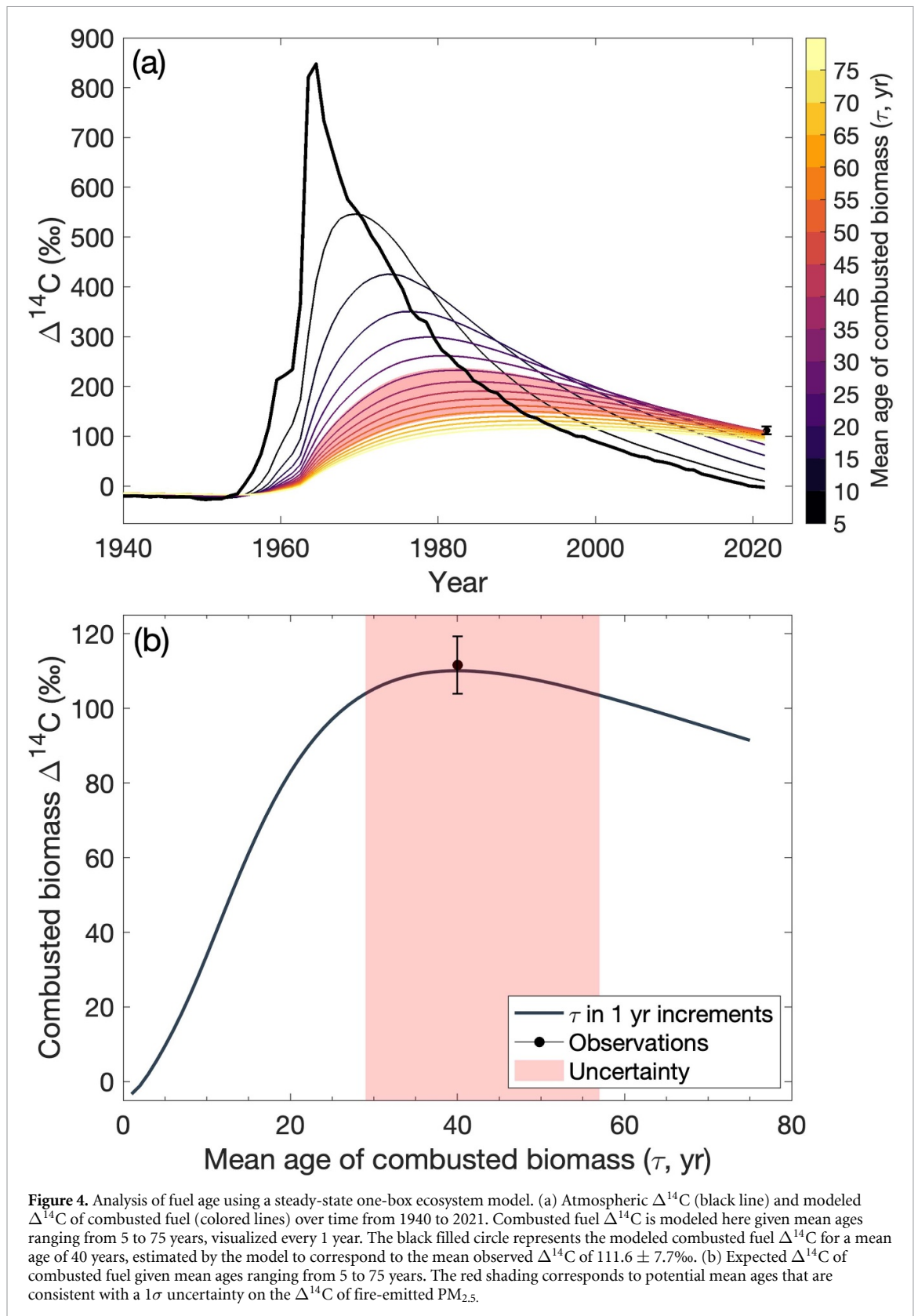


is typical of a diurnal circulation pattern in mountain regions (Kuwahata and Kondo 1989, Geerts *et al* 2008).

The trace gas and $\text{PM}_{2.5}$ time series downwind of the KNP Complex Fire were also considerably elevated relative to expected levels in the background atmosphere. For CO , initial measurements at our sampling site (1330 ppb) were more than 13 times higher than the monthly average ‘clean air’ level of 98 ppb measured at Cape Kumukahi, HI, USA in October 2021 by the Global Monitoring Laboratory of NOAA’s Earth System Research Laboratory (Petron *et al* 2022). For CH_4 , our initial measurement of 2090 ppb was 7% higher than the October 2021 average of 1945 ppb at Cape Kumukahi (Lan *et al* 2022). Initial $\text{PM}_{2.5}$ concentrations of $460 \mu\text{g m}^{-3}$ far exceeded the limits deemed safe ($35 \mu\text{g m}^{-3}$) and even hazardous ($250 \mu\text{g m}^{-3}$) by the U.S. EPA (Aguilera *et al* 2021). The high correlation among the different tracers and the elevated atmospheric concentrations relative to expected background levels (Akagi *et al* 2011, Andreae 2019) provided evidence that wildfire emissions were the dominant driver of the variations in atmospheric composition observed during our sampling campaign.

The TC concentration of our filter samples closely tracked the *in-situ* optical estimates of $\text{PM}_{2.5}$ concentration and varied between 97.5 and $556.4 \mu\text{g C m}^{-3}$ (figure 2(c)). The $\Delta^{14}\text{C}$ of TC was negative near the beginning of the sampling period (figure 2(d)), which is consistent with a substantial contribution from fossil emissions in the background atmosphere (Mouteva *et al* 2015, 2017). During the evening on 2 October, $\Delta^{14}\text{C}$ increased concurrently with the rise in trace gas mole fractions and $\text{PM}_{2.5}$ concentrations, reaching a maximum of $81.0 \pm 3.1\text{‰}$ for the sample collected between midnight and 4:00 am on 3 October. From 4:00 am to mid-afternoon on 3 October, $\Delta^{14}\text{C}$ values were relatively constant, varying between $66.8 \pm 2.0\text{‰}$ and $83.6 \pm 5.6\text{‰}$ before declining to $43.4 \pm 2.1\text{‰}$ during the last sampling interval. The $\Delta^{14}\text{C}$ of TC increased at higher $\text{PM}_{2.5}$ concentrations, suggesting that fire-emitted $\text{PM}_{2.5}$, which we expect to be enriched in ^{14}C , drove variability in emissions.

Using the Keeling plot approach described in section 2.3.2, we estimated that the mean $\Delta^{14}\text{C}$ of the wildfire end member was $111.6 \pm 7.7\text{‰}$ (figure 3). The $\Delta^{14}\text{C}$ of emissions was enriched relative to the northern hemisphere atmospheric CO_2 background



in 2021 of $-3.2 \pm 1.4\text{‰}$, indicating the combusted fuels likely accumulated over a period of many decades, during a time when the atmosphere was more enriched in bomb ^{14}C (figure 4(a)).

To further constrain the age range of the wildfire $\text{PM}_{2.5}$ emissions, we used the steady-state one-box

ecosystem model described in section 2.3.3, in which the mean transit time of the carbon is equal to its mean age. With the uncertainty range of our observed combusted fuel $\Delta^{14}\text{C}$ ($111.6 \pm 7.7\text{‰}$), we attained a best-fit for fuel age of 40 years, with an asymmetrical uncertainty range of 29–57 years, corresponding to

1σ uncertainty of the mean $\Delta^{14}\text{C}$ (figure 4(b)). In 2021, a fuel class with a relatively young mean age (5 years) would have a $\Delta^{14}\text{C}$ of 9.5‰, which is only slightly enriched relative to the contemporary atmosphere in 2021 (figure 4(a)). Needles and leaf litter may be examples of materials in this fuel class. Since these materials decompose relatively quickly, very little retain the high degree of bomb labeling from the 1950s and 1960s. As the age of fuels increases from 5 to 40 years, the predicted $\Delta^{14}\text{C}$ of combusted fuel from the model rises to approximately 110.0‰. Fuels with a 40 year mean age may encompass larger-diameter woody detritus and other woody biomass like live shrubs and small trees.

4. Discussion

The diameter of woody fuels influences the length of time required for decomposition in forest ecosystems. Fine fuels (i.e., needles, leaf litter, and small-diameter woody detritus) decompose relatively rapidly over several years. In contrast, fuels with a larger diameter decompose relatively slowly and can remain in the understory and on the forest floor for decades (Harmon 2021). Lower-intensity fires, including prescribed fires, typically consume only fine fuel classes because larger-diameter fuels generally have a higher moisture content and require more energy to ignite and support high-intensity fires (Chuvieco *et al* 2002, Gorte 2009). High rates of energy release from the consumption of large-diameter fuels, in turn, can contribute to longer flame lengths and increase probability that ground fires will jump into the overstory and develop into crown fires (Stephens *et al* 2022). High-intensity crown fires are a major concern with respect to preservation of giant sequoias because thick bark near the base of tree makes sequoias nearly impervious to ground fires, yet scorch in the upper canopy can damage foliage and more vulnerable vascular tissues (Shive *et al* 2022).

Our $\Delta^{14}\text{C}$ measurements provide evidence that the KNP Complex Fire burned through larger-diameter fuels, likely with a considerably higher intensity than what would be expected for surface fires. It is also possible that the combustion of deeper organic soil (Pellegrini *et al* 2021), which has a similar mean age to the woody detritus in some forests (Mouteva *et al* 2015), also contributed to emissions. However, our study does not include depth of burn measurements, which would allow us to apportion the relative contributions from woody detritus and soil. Still, our measurements are broadly consistent with previous studies documenting how the accumulation of fuel in California's coniferous forests (including the buildup of shrubs, small trees, and woody detritus on multi-decadal timescales) contributes to high fire intensity (Miller *et al* 2009b, Safford and Stevens 2017, Stevens *et al* 2017b). Notably, the KNP Complex Fire led to the mortality

of about 5900 giant sequoias, meaning that 3%–5% of all giant sequoias in the Sierra Nevada mountains were killed or are expected to die within 5 years (Stephenson and Brigham 2021). This compounds giant sequoia mortality from the 2020 Castle Fire, which killed an estimated 10%–14% of large giant sequoias (Stephenson and Brigham 2021). The native range of giant sequoias does not extend beyond the western slope of the Sierra Nevada, therefore a loss of approximately 15% in such a short period is a major threat to this endangered species.

Fuel treatments, including mechanical thinning and prescribed fire, have historically been used to decrease fuel loads in forests. Legislation was recently passed in California that will expand the use of prescribed fire across the state with a goal of one million acres treated per year by 2025 (California Wildfire and Forest Resilience Task Force 2022). If they are successful, we expect fuel treatments to gradually reduce the mean age of combusted fuels because understory vegetation and larger-diameter woody detritus should be removed (Harmon 2021). Regional PM sampling during periods with prescribed fire might be an effective way to monitor the success of this program. Specifically, after a sustained effort, the $\Delta^{14}\text{C}$ of combusted fuel should more closely match the contemporary atmosphere because finer fuel classes have younger mean ages. Eventually, wildfires would also be expected to have lower intensities and more closely track the $\Delta^{14}\text{C}$ of atmospheric CO_2 .

Apart from evaluating the effectiveness of prescribed burning, PM $\Delta^{14}\text{C}$ monitoring in California may be helpful for understanding the role of wildfire in influencing air quality across the state. For instance, the San Joaquin Valley of California is a serious non-attainment area for $\text{PM}_{2.5}$ and other pollutants with adverse health effects. It often exceeds both state and national air quality standards for harmful pollutants (Huang *et al* 2021). Pollution in the San Joaquin Valley is primarily anthropogenic due to both local emissions and those transported from surrounding urban areas, but wildfires play a variable and often significant role in elevated pollutant levels (Schweizer and Cisneros 2017, Burke *et al* 2021, Frausto-Vicencio *et al* 2023). Disentangling contributions to observed $\text{PM}_{2.5}$ levels from prescribed fire, wildfire, and urban sources will be critical for creating effective policy to improve air quality in the San Joaquin Valley and simultaneously meet the State's forest management goals.

Future directions for this work include building a longer time series of observations from multiple fires, which will provide information about a broader range of burning conditions. The length of our time series was constrained by rapidly changing conditions and challenges securing a safe sampling location that was both near the smoke and outside of the mandatory evacuation zone. Future analyses should be conducted over longer sampling intervals on a variety of wildland fire types, including grass and shrub

fires and prescribed fire, to more broadly understand the effects of climate, fuel, and fuel treatments on the composition of PM emissions across California and other fire-prone forests. Fire emissions contain many carbonaceous components (Olsen *et al* 2020), so another important research direction is to simultaneously measure the $\Delta^{14}\text{C}$ of elemental and organic carbon (EC and OC) $\text{PM}_{2.5}$ fractions and carbon-containing trace gases (CO and CO_2) to understand better the linkages between fuel age (and type), flaming and smoldering combustion, and the composition of fire emissions. In past work, for example, fire-emitted EC has been shown to have higher levels of $\Delta^{14}\text{C}$ than OC, likely due to a different mixture of fuels (Mouteva *et al* 2015).

5. Conclusions

In this study, we measured the $\Delta^{14}\text{C}$ of $\text{PM}_{2.5}$ from the KNP Complex Fire and used these observations to infer that fuel buildup over multiple decades was a dominant contributor to $\text{PM}_{2.5}$ emissions in smoke. Our analysis is consistent with past work showing that cessation of Indigenous burning practices and implementation of fire suppression in the Sierra Nevada mountains are important contributors to recent increases in fire intensity. We also propose that our measurement techniques can be used to assess the efficacy of prescribed fire and other fuel treatments planned for California in the near future and to identify fire impacts on air quality in remote urban areas. Altogether, fuel management and an enhanced understanding of emissions associated with California's wildfires can help mitigate their social, economic, and ecosystem impacts.

Data availability statement


The data that support the findings of this study are openly available at the following URL/DOI: <https://doi.org/10.7280/D1498P> (Odwuor 2023).

Acknowledgments

This work was conducted on the unceded lands of the Mono (Monache), Yokut, Tübatulabal, Paiute, and Western Shoshone people (National Park Service 2021). This material is based upon work supported by the National Science Foundation Graduate Research Fellowship under Grant No. DGE-2039655 to AO. J T R received funding support from the NASA's Modeling, Analysis, and Prediction (MAP) and Earth Information System—Fire research programs and the U.S. Department of Energy Office of Science's RUBISCO Science Focus Area. Funding from the Ralph J and Carol. M Cicerone Chair in the Department of Earth System Science supported the field campaign and laboratory measurements.

We thank the KCCAMS staff for supporting the elemental and isotopic analyses and A Ocampo and C McCormick for assisting with data collection.

ORCID iDs

A Odwuor  <https://orcid.org/0000-0001-9104-5025>
 C C Yañez  <https://orcid.org/0000-0003-1521-2906>
 Y Chen  <https://orcid.org/0000-0002-0993-7081>
 F M Hopkins  <https://orcid.org/0000-0002-6110-7675>
 A Moreno  <https://orcid.org/0000-0001-7598-2764>
 X Xu  <https://orcid.org/0000-0003-3678-2748>
 C I Czimeczik  <https://orcid.org/0000-0002-8251-6603>
 J T Randerson  <https://orcid.org/0000-0001-6559-7387>

References

- Abatzoglou J T *et al* 2021 Projected increases in western US forest fire despite growing fuel constraints *Commun. Earth Environ.* **2** 227
- Aguilera R, Corringham T, Gershunov A and Benmarhnia T 2021 Wildfire smoke impacts respiratory health more than fine particles from other sources: observational evidence from Southern California *Nat. Commun.* **12** 1493
- Akagi S K, Yokelson R J, Wiedinmyer C, Alvarado M J, Reid J S, Karl T, Crouse J D and Wennberg P O 2011 Emission factors for open and domestic biomass burning for use in atmospheric models *Atmos. Chem. Phys.* **11** 4039–72
- Andreae M 2019 Emission of trace gases and aerosols from biomass burning. Global biogeochemical *Atmos. Chem. Phys.* **15** 955–66
- Burke M, Driscoll A, Heft-Neal S, Xue J, Burney J and Wara M 2021 The changing risk and burden of wildfire in the United States *Proc. Natl Acad. Sci. USA* **118** e2011048118
- California Department of Forestry and Fire Protection 2022a *Emergency Fund Fire Suppression Expenditures* (available at: www.fire.ca.gov/media/px5lnaaw/suppressioncostsonpage1.pdf) (Accessed 20 February 2023)
- California Department of Forestry and Fire Protection 2022b *Fire and Resource Assessment Program Fire Perimeters* (available at: <https://frap.fire.ca.gov/mapping/gis-data/on>) (Accessed 20 February 2023)
- California Wildfire and Forest Resilience Task Force 2022 *California's Strategic Plan for Expanding the Use of Beneficial Fire* (available at: www.fire.ca.gov/media/xccjppjmc/californias-strategic-plan-for-expanding-the-use-of-beneficial-fire-march-16_2022.pdf) (Accessed 20 February 2023)
- Chen Y *et al* 2022 California wildfire spread derived using VIIRS satellite observations and an object-based tracking system *Sci. Data* **9** 249
- Chuvieco E, Riaño D, Aguado I and Cocero D 2002 Estimation of fuel moisture content from multitemporal analysis of landsat thematic mapper reflectance data: applications in fire danger assessment *Int. J. Remote Sens.* **23** 2145–62
- Dennison P E, Brewer S C, Arnold J D and Moritz M A 2014 Large wildfire trends in the western United States, 1984–2011 *Geophys. Res. Lett.* **41** 6413–9
- Foster D E, Battles J J, Collins B M, York R A and Stephens S L 2020 Potential wildfire and carbon stability in frequent-fire forests in the Sierra Nevada: trade-offs from a long-term study *Ecosphere* **11** e03198
- Frausto-Vicencio I, Heerah S, Meyer A G, Parker H A, Dubey M and Hopkins F M 2023 Ground solar absorption observations of total column CO , CO_2 , CH_4 , and aerosol

- optical depth from California's Sequoia Lightning Complex Fire: emission factors and modified combustion efficiency at large scales *Atmos. Chem. Phys. Discuss.* **23** 4521–43
- Geerts B, Miao Q and Demko J C 2008 Pressure perturbations and upslope flow over a heated, isolated mountain *Mon. Weather Rev.* **136** 4272–88
- Gorte R W 2009 Wildfire fuels and fuel reduction (Report no. R40811) *Congressional Research Service, Library of Congress* pp 1–16 (available at: <https://crsreports.congress.gov/product/pdf/R/R40811/12on>) (Accessed 20 February 2023)
- Gutierrez A A, Hantson S, Langenbrunner B, Chen B, Jin Y, Goulden M L and Randerson J T 2021 Wildfire response to changing daily temperature extremes in California's Sierra Nevada *Sci. Adv.* **7** e2905–11
- Hagmann R K et al 2021 Evidence for widespread changes in the structure, composition, and fire regimes of western North American forests *Ecol. Appl.* **31** e0243
- Harmon M E 2021 The role of woody detritus in biogeochemical cycles: past, present, and future *Biogeochemistry* **154** 349–69
- Higuera P E and Abatzoglou J T 2021 Record-setting climate enabled the extraordinary 2020 fire season in the western United States *Glob. Change Biol.* **27** 1–2
- Hopkins F M, Ehleringer J R, Bush S E, Duren R M, Miller C E, Lai C-T, Hsu Y-K, Carranza V and Randerson J T 2016 Mitigation of methane emissions in cities: how new measurements and partnerships can contribute to emissions reduction strategies *Earth's Future* **4** 408–25
- Hua Q et al 2022 Atmospheric radiocarbon for the period 1950–2019 *Radiocarbon* **64** 723–45
- Huang L, Sun J, Jin L, Brown N J and Hu J 2021 Strategies to reduce PM_{2.5} and O₃ together during late summer and early fall in San Joaquin Valley, California *Atmos. Res.* **258** 105633
- Keeling C D 1958 The concentration and isotopic abundances of atmospheric carbon dioxide in rural areas *Geochim. Cosmochim. Acta* **13** 322–34
- Key C H and Benson N C 2006 Landscape assessment (LA) sampling and analysis methods *FIREMON: Fire Effects Monitoring and Inventory System* RMRS-GTR-164 ed D C Lutes, R E Keane, J F Caratti, C H Key, N C Benson, S Sutherland and L J Gangi (U.S. Department of Agriculture Forest Service, Rocky Mountain Research Station)
- Kochi I, Donovan G H, Champ P A and Loomis J B 2010 The economic cost of adverse health effects from wildfire-smoke exposure: a review *Int. J. Wildland Fire* **19** 803–17
- Kuwagata T and Kondo J 1989 Observation and modeling of thermally induced upslope flow *Bound.-Layer Meteorol.* **49** 265–93
- Lan X, Dlugokencky E J, Mund J W, Crotwell A M, Crotwell M J, Moglia E, Madronich M, Neff D and Thoning K W 2022 Atmospheric methane dry air mole fractions from the NOAA GML carbon cycle cooperative global air sampling network, 1983–2021 Version: 2022–11–21 (<https://doi.org/10.15138/VNCZ-M766>)
- Levin I, Naegler T, Kromer B, Diehl M, Francey R J, Gomez-Pelaez A J, Steele L P, Wagenbach D, Weller R and Worthy D E 2010 Observations and modelling of the global distribution and long-term trend of atmospheric ¹⁴CO₂ *Tellus B* **62** 26–46
- McKelvey K S and Busse K K 1996 Twentieth-century fire patterns on forest service lands *Sierra Nevada Ecosystem Project: Final Report to Congress*, II pp 1119–38
- Miller J D, Knapp E E, Key C H, Skinner C N, Isbell C J, Creasy R M and Sherlock J W 2009a Calibration and validation of the relative differenced normalized burn ratio (RdNBR) to three measures of fire severity in the Sierra Nevada and Klamath mountains, California, USA *Remote Sens. Environ.* **113** 645–56
- Miller J D, Safford H D, Crimmins M and Thode A E 2009b Quantitative evidence for increasing forest fire severity in the Sierra Nevada and southern Cascade mountains, California and Nevada, USA *Ecosystems* **12** 16–32
- Mouteva G O et al 2015 Black carbon aerosol dynamics and isotopic composition in Alaska linked with boreal fire emissions and depth of burn in organic soils *Glob. Biogeochem. Cycles* **29** 1977–2000
- Mouteva G O, Randerson J T, Fahrni S M, Bush S E, Ehleringer J R, Xu X, Santos G M, Kuprov R, Schichtel B A and Czimeczik C I 2017 Using radiocarbon to constrain black and organic carbon aerosol sources in Salt Lake City J. *Geophys. Res.* **122** 9843–57
- National Park Service and Sequoia and Kings Canyon National Parks 2017 *Sequoia Groves of the Sierra Nevada California* (available at: <https://irma.nps.gov/DataStore/Reference/Profile/2259632on>) (Accessed 20 February 2023)
- National Park Service 2021 *Native Americans of the Southern Sierra* (available at: www.nps.gov/seki/learn/historyculture/native-americans.htm) (Accessed 21 February 2023)
- Nydal R 1963 Increase in radiocarbon from the most recent series of thermonuclear tests *Nature* **200** 212–4
- Odwuor A 2023 Dryad Dataset (<https://doi.org/10.7280/D1498P>)
- Olsen Y, Nøjgaard J K, Olesen H R, Brandt J, Sigsgaard T, Pryor S C and Hertel O 2020 Emissions and source allocation of carbonaceous air pollutants from wood stoves in developed countries: a review *Atmos. Pollut. Res.* **11** 234–51
- Pataki D E, Ehleringer J R, Flanagan L B, Yakir D, Bowling D R, Still C J, Buchmann N, Kaplan J O and Berry J A 2003 The application and interpretation of Keeling plots in terrestrial carbon cycle research *Glob. Biogeochem. Cycles* **17** 1022
- Pausas J G and Keeley J E 2019 Wildfires as an ecosystem service *Front. Ecol. Environ.* **17** 289–95
- Pellegrini A F, Caprio A C, Georgiou K, Finnegan C, Hobbie S E, Hatten J A and Jackson R B 2021 Low-intensity frequent fires in coniferous forests transform soil organic matter in ways that may offset ecosystem carbon losses *Glob. Change Biol.* **27** 3810–23
- Petron G, Crotwell A M, Crotwell M J, Dlugokencky E, Madronich M, Moglia E, Neff D, Thoning K, Wolter S and Mund J W 2022 Atmospheric carbon monoxide dry air mole fractions from the NOAA GML carbon cycle cooperative global air sampling network, 1988–2021 Version: 2022–07–28 (<https://doi.org/10.15138/33bv-s284>)
- Reid C E, Brauer M, Johnston F H, Jerrett M, Balmes J R and Elliott C T 2016 Critical review of health impacts of wildfire smoke exposure *Environ. Health Perspect.* **124** 1334–43
- Safford H D, Paulson A K, Steel Z L, Young D J N, Wayman R B and Varner M 2022 The 2020 California fire season: a year like no other, a return to the past or a harbinger of the future? *Glob. Ecol. Biogeogr.* **31** 2005–25
- Safford H D and Stevens J T 2017 Natural Range of Variation for Yellow Pine and Mixed-conifer Forests in the Sierra Nevada, Southern Cascades, and Modoc and Inyo National Forests, California, USA *General Technical Report—Pacific Southwest Research Station, USDA Forest Service PSW-GTR-256*, (PSW-GTR-256) p 229
- Schweizer D W and Cisneros R 2017 Forest fire policy: change conventional thinking of smoke management to prioritize long-term air quality and public health *Air Qual. Atmos. Health* **10** 33–36
- Shive K L, Wuenschel A, Hardlund L J, Morris S, Meyer M D and Hood S M 2022 Ancient trees and modern wildfires: declining resilience to wildfire in the highly fire-adapted giant sequoia *For. Ecol. Manage.* **511** 120110
- Stephens S L et al 2009 Fire treatment effects on vegetation structure, fuels, and potential fire severity in western U.S. forests *Ecol. Appl.* **19** 305–20
- Stephens S L, Bernal A A, Collins B M, Finney M A, Lautenberger C and Saah D 2022 Mass fire behavior created by extensive tree mortality and high tree density not predicted by operational fire behavior models in the southern Sierra Nevada *For. Ecol. Manage.* **518** 120258
- Stephenson N and Brigham C 2021 Preliminary estimates of sequoia mortality in the 2020 Castle Fire (National Park Service) pp 1–32

- Stevens J T 2017a Scale-dependent effects of post-fire canopy cover on snowpack depth in montane coniferous forests *Ecol. Appl.* **27** 1888–900
- Stevens J T et al 2021 Tamm review: postfire landscape management in frequent-fire conifer forests of the southwestern United States *For. Ecol. Manage.* **502** 119678
- Stevens J T, Collins B M, Miller J D, North M P and Stephens S L 2017b Changing spatial patterns of stand-replacing fire in California conifer forests *For. Ecol. Manage.* **406** 28–36
- Stuvier M and Polach H A 1977 Discussion: reporting of ^{14}C data *Radiocarbon* **19** 355–63
- Swetnam T W et al 2009 Multi-millennial fire history of the giant forest *Fire Ecology* (Sequoia National Park) vol 5 pp 120–50
- Swetnam W 1993 Fire history and climate change in giant sequoia groves *Science* **262** 885–9
- Taylor A H, Trouet V, Skinner C N and Stephens S 2016 Socioecological transitions trigger fire regime shifts and modulate fire-climate interactions in the Sierra Nevada, USA, 1600–2015 CE *Proc. Natl Acad. Sci. USA* **113** 13684–9
- Tubbesing C L, Martinez D J and Smith J 2021 Prioritizing forest health investments: recommendations from the science advisory panel to the forest management task force
- Walker B D and Xu X 2019 An improved method for the sealed-tube zinc graphitization of microgram carbon samples and ^{14}C AMS measurement *Nucl. Instrum. Methods Phys. Res. B* **438** 58–65
- Wang D et al 2021 Economic footprint of California wildfires in 2018 *Nat. Sustain.* **4** 252–60
- Wiggins E B, Czimczik C I, Santos G M, Chen Y, Xu X, Holden S R, Randerson J T, Harvey C F, Kai F M and Yu L E 2018 Smoke radiocarbon measurements from Indonesian fires provide evidence for burning of millennia-aged peat *Proc. Natl Acad. Sci. USA* **115** 12419–24
- Williams A P, Abatzoglou J T, Gershunov A, Guzman-Morales J, Bishop D A, Balch J K and Lettenmaier D P 2019 Observed impacts of anthropogenic climate change on wildfire in California *Earth's Future* **7** 892–910
- Wu T, Kim Y S and Hurteau M D 2011 Investing in natural capital: using economic incentives to overcome barriers to forest restoration *Restor. Ecol.* **19** 441–5
- Yañez C C, Hopkins F M, Xu X, Tavares J E, Welch A and Czimczik C I 2022 Reductions in California's urban fossil fuel CO_2 emissions during the COVID-19 pandemic *AGU Adv.* **3** e2022AV000732